Dose specification for ^{192}Ir high dose rate brachytherapy in terms of dose-to-water-in-medium and dose-to-medium-in-medium

2015 Phys. Med. Biol. 60 4565

(http://iopscience.iop.org/0031-9155/60/11/4565)

IOP Publishing | Institute of Physics and Engineering in Medicine Physics in Medicine & Biology

Phys. Med. Biol. **60** (2015) 4565–4579 doi:10.1088/0031-9155/60/11/4565

Dose specification for ^{192}Ir high dose rate brachytherapy in terms of dose-to-water-in-medium and dose-to-medium-in-medium

Gabriel Paiva Fonseca[1,2], Åsa Carlsson Tedgren[3,4], Brigitte Reniers[2,5], Josef Nilsson[3], Maria Persson[3], Hélio Yoriyaz[1] and Frank Verhaegen[2,6]

[1] Instituto de Pesquisas Energéticas e Nucleares—IPEN-CNEN/SP, São Paulo, Brazil
[2] Department of Radiation Oncology (MAASTRO), GROW School for Oncology and Developmental Biology, Maastricht University Medical Center, Maastricht 6201 BN, The Netherlands
[3] Section of Radiotherapy Physics and Engineering, Department of Medical Physics, Karolinska University Hospital, Stockholm, Sweden
[4] Medical Radiation Physics, Department of Medical and Health Sciences (IMH), Linköping University, Linköping, Sweden
[5] Research group NuTeC, CMK, Hasselt University, Agoralaan Gebouw H, B-3590 Diepenbeek, Belgium
[6] Medical Physics Unit, Department of Oncology, McGill University, Montréal, Québec H3G 1A4, Canada

E-mail: frank.verhaegen@maastro.nl

Received 19 February 2015, revised 7 April 2015
Accepted for publication 21 April 2015
Published 26 May 2015

Abstract

Dose calculation in high dose rate brachytherapy with ^{192}Ir is usually based on the TG-43U1 protocol where all media are considered to be water. Several dose calculation algorithms have been developed that are capable of handling heterogeneities with two possibilities to report dose: dose-to-medium-in-medium ($D_{m,m}$) and dose-to-water-in-medium ($D_{w,m}$). The relation between $D_{m,m}$ and $D_{w,m}$ for ^{192}Ir is the main goal of this study, in particular the dependence of $D_{w,m}$ on the dose calculation approach using either large cavity theory (LCT) or small cavity theory (SCT). A head and neck case was selected due to the presence of media with a large range of atomic numbers relevant to tissues and mass densities such as air, soft tissues and bone interfaces. This case was simulated using a Monte Carlo (MC) code to score: $D_{m,m}$, $D_{w,m}$ (LCT), mean photon energy and photon fluence. $D_{w,m}$ (SCT) was derived from MC simulations using the ratio between the unrestricted collisional stopping power of the actual medium and water. Differences between $D_{m,m}$ and $D_{w,m}$ (SCT or LCT) can be negligible (<1%) for some tissues e.g. muscle and

significant for other tissues with differences of up to 14% for bone. Using SCT or LCT approaches leads to differences between $D_{w,m}$ (SCT) and $D_{w,m}$ (LCT) up to 29% for bone and 36% for teeth. The mean photon energy distribution ranges from 222 keV up to 356 keV. However, results obtained using mean photon energies are not equivalent to the ones obtained using the full, local photon spectrum. This work concludes that it is essential that brachytherapy studies clearly report the dose quantity. It further shows that while differences between $D_{m,m}$ and $D_{w,m}$ (SCT) mainly depend on tissue type, differences between $D_{m,m}$ and $D_{w,m}$ (LCT) are, in addition, significantly dependent on the local photon energy fluence spectrum which varies with distance to implanted sources.

Keywords: brachytherapy, ^{192}Ir, dose-to-water-in-medium, dose-to-medium-in-medium

(Some figures may appear in colour only in the online journal)

1. Introduction

Dose calculation in high dose rate (HDR) brachytherapy with the ^{192}Ir isotope is usually based on the TG-43U1 protocol (Nath *et al* 1995, Rivard *et al* 2004) where all media are considered to be water. Clinical brachytherapy treatment planning systems (TPS) therefore create brachytherapy treatment plans based on dose distributions in water ($D_{w,w}$—TG-43), and were not capable of handling non-water heterogeneities. Recently, several model based dose calculation algorithms (MBDCA) have been developed that are capable of handling heterogeneities. Examples of such dose engines include graphical user interfaces coupled with general-purpose Monte Carlo (MC) codes (Fonseca *et al* 2014, Poon *et al* 2008), MC codes optimized for brachytherapy (Taylor *et al* 2007, Thomson *et al* 2010, Afsharpour *et al* 2012) and two commercial systems, Acuros™ (Transpire Inc., Gig Harbor, WA) (Petrokokkinos *et al* 2011, Lloyd and Ansbacher 2013, Mikell *et al* 2013), available in BrachyVision™ (Varian Medical Systems, Inc., Palo Alto, CA), and the Advanced Calculation Engine (ACE) (Nucletron—an Elekta Company, Veenendaal, the Netherlands) (Carlsson Tedgren and Ahnesjo 2003, 2008, 2000, Ahnesjo 1989, Russell *et al* 2005).

The recent AAPM Task Group Report 186 (Beaulieu *et al* 2012) (AAPM TG-186) provides guidelines to take patient and applicator non-water materials into account and also describes the different dose reporting quantities possible: dose-to-medium-in-medium ($D_{m,m}$), and dose-to-water-in-medium ($D_{w,m}$). Differences between dose reporting in terms of $D_{m,m}$ and $D_{w,m}$ have been discussed in the literature (Chetty *et al* 2007, Ma and Li 2011, Beaulieu *et al* 2012) with arguments in favor and against both quantities.

The way to define $D_{w,m}$ depends on assumptions in the employed cavity theory regarding the cavity dimensions compared to the ranges of secondary electrons. Absorbed dose can be calculated to a small water cavity of cellular dimensions or to a large water cavity of dimensions similar to the Computed Tomography (CT) defined voxels used in MBDCA treatment planning. Large Cavity Theory (LCT) uses the ratio of mass-energy absorption coefficients (medium/water), $(\mu_{en}/\rho)^{m}_{w}$, assuming charged particle equilibrium (CPE) for the cavity of interest (Landry *et al* 2011, Rivard *et al* 2010a). Small Cavity Theory (SCT) uses the ratio between mass stopping power (medium/water), $(S/\rho)^{m}_{w}$, for Bragg-Gray cavities with dimensions much smaller than the secondary electron ranges (Beaulieu *et al* 2012, Carlsson Tedgren and Alm Carlsson 2013).

In external beam radiotherapy (EBRT), where ranges of secondary electrons are substantially longer than in brachytherapy, the cavity has been assumed to be small and conversion between $D_{m,m}$ and $D_{w,m}$ is made through ratios of unrestricted mass collision stopping power, water to medium (Liu *et al* 2002, Chetty *et al* 2007, Ma and Li 2011). Recently, Andreo revisited this topic in detail for EBRT (Andreo 2015). To define a cavity as small, large or even intermediate sized becomes complex in brachytherapy as ranges of secondary electrons from low energy photons (<50 keV) are comparable to the cellular dimensions (few μm) (Beaulieu *et al* 2012). Carlsson Tedgren and Alm Carlsson evaluated, using the Burlin theory, when cavity dimensions ranging from 1 nm to 10 mm could be assumed large, small or intermediate at various photon energies of relevance to brachytherapy. Assumed dimensions of the water cavity could be of interest to evaluate the correlation between dose reporting quantities and biological effects (Carlsson Tedgren and Alm Carlsson 2013, Thomson *et al* 2013). Lindborg *et al* recently found the clinical radiobiological effect (RBE) for radiotherapy modalities ranging from kV x-rays to protons and heavier ions to correlate with the microdosimetric quantity mean linear energy when the latter was evaluated in volumes of nm dimensions (Lindborg *et al* 2013). The reporting dose quantities for a cell nucleus ($D_{n,m}$) of μm dimension, $D_{w,m}$ and $D_{m,m}$ were evaluated by Enger *et al* for different cell nucleus compositions (Enger *et al* 2012).

AAPM TG-186 recommends that $D_{m,m}$ should always be reported and states that more studies are necessary on how to calculate $D_{w,m}$ before any definitive recommendation can be made. Differences between the quantities $D_{m,m}$ and $D_{w,m}$ (LCT) are considerably smaller for the ^{192}Ir spectrum (Rivard *et al* 2010b) than for low photon energy (<50 keV) isotopes due to its relatively high photon energies (initial mean energy $\approx$ 355 keV). The mean photon energies described in this work were weighted over the photon fluence. Figure 1(a) shows how ratios of mass-energy absorption coefficients (μ_{en}/ρ) between tissues and water increase at lower photon energies. However, as the photon spectrum changes away from the implanted sources due to the combined effect of attenuation of primary- and buildup of scattered-photons, larger differences between $D_{m,m}$ and $D_{w,m}$ (LCT) should occur also around an ^{192}Ir implant. Differences between $D_{m,m}$ and $D_{w,m}$ (SCT) are likely to be much less relevant since ratios of mass collision stopping powers $(S_{col}/\rho)^{m}_{w}$ are approximately independent of the energy (see figure 1(b)).

The aim of this work is to evaluate $D_{w,m}$ values obtained using SCT and LCT in a head and neck patient treated with HDR (high dose rate) ^{192}Ir. The head and neck case was selected due to the presence of air, soft tissues and bone interfaces. The photon spectrum and dose reporting approaches in various locations in and outside of the brachytherapy implant will be studied in detail.

2. Materials and methods

This section describes the evaluated clinical case, simulation parameters and the methodology employed to convert $D_{m,m}$ to $D_{w,m}$ using SCT and LCT.

2.1. Clinical case

The treatment plan for an interstitial clinical head and neck case was made with a CT image set consisting of 80 slices with 512 × 512 voxels (0.39 × 0.39 × 2.00 mm^3). Dose distributions were calculated for a HDR ^{192}Ir microSelectron v.2 (Nucletron) source (Daskalov *et al* 1998, Taylor and Rogers 2008) and six plastic catheters with a total of 99 dwell positions. 25 CT voxels were visually selected to evaluate the photon spectrum at several regions of the irradiated volume occupied by different materials and at different distances from implanted

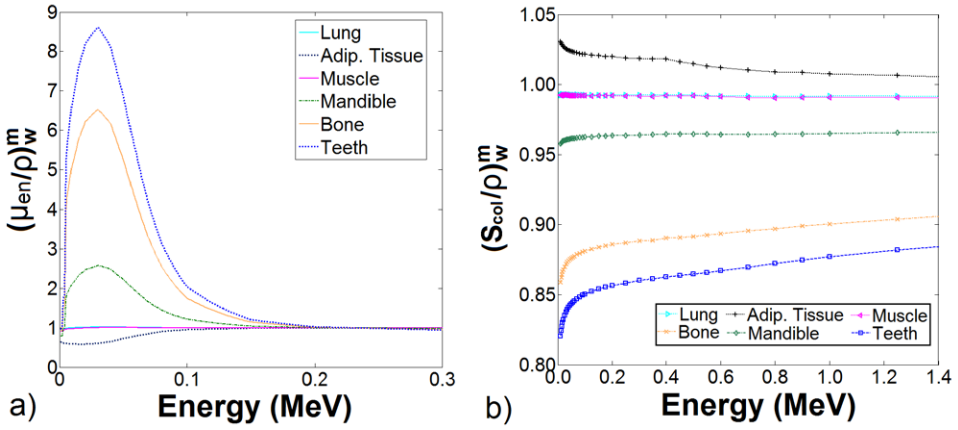

Figure 1. (a) mass energy absorption coefficients (μ_{en}/ρ) of various human tissues relative to water coefficients. Values for elemental media obtained from NIST (Berger *et al* 2005b) and combined into human tissues using the mass-fraction of each element (ICRP 2009). (b) Unrestricted mass collision stopping power (S_{col}/ρ) ratios of various human tissues relative to those for water. Values obtained using ESTAR database considering the mass-fraction of each element (Berger 2005a).

sources. The patient CT geometry and the location of the 25 voxels for which the photon spectrum was scored (see the next section) are shown in figure 2.

2.2. Monte Carlo simulations

The CT images were segmented using auxiliary software (Fonseca *et al* 2014) to create three voxel phantoms including: I—a water (ρ = 1 g cm^{-3}) and air (ρ = 0.0012 g cm^{-3}) phantom; II—a water and air phantom with mass densities obtained from a calibrated CT image; III—a phantom with proper tissue compositions (adipose tissue, muscle and bone) (ICRP 2009), with mass densities obtained from a calibrated CT image. The regions with air are the same for all models adopted so henceforward this material will not be mentioned anymore when referring to the described phantoms. These phantoms were employed to evaluate the effect of different approaches/simplifications that can be easily adopted by MC users. Moreover, $D_{w,w}$ values obtained with phantom II were compared (data not shown) against $D_{w,m}$ (LCT) and $D_{m,m}$ values obtained with phantom III since using phantom II is simpler, but may still provide reasonable results. The numbers (I, II and III) were used in the next sections to distinguish the three different approaches.

Simulations were performed with the MC code MCNP6 (Monte Carlo n-Particle, version 1.0) (Goorley 2012, Goorley *et al* 2013) for the three phantoms, scoring in all voxels the mean photon energy per voxel, $D_{w,m}$ (LCT) and $D_{m,m}$ and for the 25 selected voxels the full photon energy spectra with a 1 keV resolution (figure 2). $D_{w,m}$ (LCT) and $D_{m,m}$ values were obtained using a track length estimator (tally F6) assuming CPE conditions so secondary electrons were not transported (see next section). Mass-energy absorption coefficients ($\mu_{en/\rho}$) from the National Institute of Standards and Technology (NIST) (Berger 2005b) for either water or medium were employed to convert photon energy fluence to collision kerma (equal to absorbed dose under CPE). MCNP6 uses the ENDF/B cross section photon library (White 2003, Hughes 2013), which is consistent with the NIST database (Carron 2006). In addition, we verified this scoring the dose delivered from several photon energy spectra, within the ^{192}Ir

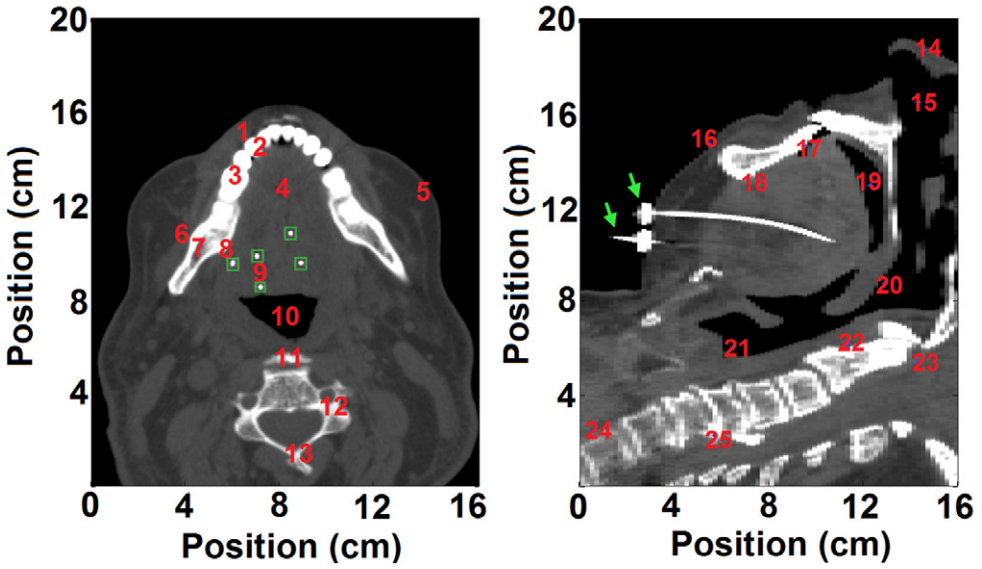

Figure 2. Axial and sagittal view of the evaluated head and neck clinical case. The numbers indicate voxels positions where the photon spectrum was scored. Green arrows and squares were added to show the catheters positions (five of the six catheters can be visualized).

photon energy range, to spherical targets of different materials. Differences (data not shown) between values obtained with MCNP6 and the ones calculated using $\mu_{en/\rho}$ from NIST are within 0.05% for all the tissues evaluated in this work.

In addition, $D_{m,m}$ values were calculated transporting secondary electrons and using a pulse height tally (F8) to verify $D_{m,m}$ obtained with a track length tally F6 to study the validity of the CPE approximation on the dosimetry (and thus on using a track length estimator for this kind of geometries) on the current dose calculation voxel grid. Earlier investigations confirmed the validity of CPE using even smaller voxels ($0.1 \times 0.1 \times 0.1\,mm^3$) (Ballester *et al* 2009), but studied the problem around a brachytherapy source positioned in pure water to estimate the importance of modelling charged particles emitted in the source decay. CPE conditions are achieved for the ^{192}Ir spectrum for distances greater than 2 mm from the source (Wang and Li 2002, Ballester *et al* 2009). However, breakdown of CPE can occur near material boundaries (Rivard *et al* 2009). The effect of the interfaces between different materials and their influence on the CPE assumption has not been studied before in a CT defined phantom with voxel dimensions as those adopted in this study.

The geometry of the microSelectron v.2 source (Daskalov *et al* 1998) was simulated with photon emission from an ^{192}Ir spectrum from the National Nuclear Data Center (NNDC) (Rivard *et al* 2010b, Baglin 2012) to generate a phase space file. Photons were transported down to an energy cut-off of 1 keV, using the MCPLIB84 photon cross-section library (Chadwick 2012), and secondary electrons were transported down to an energy cut-off of 50 keV (only for the simulation using a pulse height tally (F8)). This approach does not introduce significant uncertainties since 50 keV electrons have a residual range of 0.04 mm in water which is almost ten times shorter than the smallest voxel dimension,(Berger 2005a) and bremsstrahlung production below 50 keV in water and low atomic number material is negligible. The number of primary photons was set to 1 billion (10^9) for the mean energy

simulation (uncertainty <4% Type A $\pm 1\sigma$), 10 billion for the track length and photon spectrum simulations (uncertainty <1% Type A $\pm 1\sigma$), and 30 billion for pulse height tally simulation (uncertainty <4.5% Type A $\pm 1\sigma$).

Under CPE conditions dose values are approximated by collision kerma (and even by total kerma in low atomic number materials where bremsstrahlung is negligible) and can be obtained by multiplying the energy fluence ($E.\Phi_E$) by $\mu_{en/\rho}$ as described in equation(1). Photon fluence values were scored for N energy bins (i) with 1 keV resolution using MCNP6. This methodology is efficient since the number of tracks crossing a voxel is much higher than the number of interactions in it and leads to accurate results within the brachytherapy energy range for mm-sized voxels (Rivard *et al* 2006, Taylor and Rogers 2008, White *et al* 2014). This approach is followed in the first MC simulation (track length) mentioned above.

$$D \approx \sum_{i=1}^{N} \left[\Phi_{E_{i\,(m)}}.E_i.\left(\frac{\mu_{en}}{\rho}\right)_{(\mathbf{w}\ or\ \mathbf{m})} \right] \tag{1}$$

Pulse height tallies (F8) are analogous estimators (Williamson 1987) (like a physical detector) scoring the energy deposited per interaction inside of the scoring volume. It is an accurate method, even without electronic equilibrium, with the penalty of being statistically much less efficient than track length tallies. $D_{m,m}$ values including effects of electron transport were obtained simulating the whole CT geometry. However, dose values were scored only for one sagittal slice to reduce the simulation time since it increases with the number of scoring volumes, which can make simulations impractical.

2.3. $D_{w,m}$ (SCT and LCT) and $D_{m,m}$ values for several tissues

$D_{w,m}$ (LCT), $D_{m,m}$ and mean photon energy values were obtained for several human tissues from ICRP Report 110 (ICRP 2009) (prostate, lung, adipose tissue, breast, skin, bladder, muscle, cartilage, mandible spongiosa, bone and teeth) with the full photon spectrum obtained at the 25 evaluated voxels. The contribution of separate parts of the photon spectrum to the total dose in each voxel was obtained by dividing the spectrum in 50 keV bins and calculating the percentage of the total dose from each bin.

$D_{w,m}$ (SCT) were obtained for each material assuming $(S_{col}/\rho)^{m}_{w}$ to be independent of the photon spectrum (figure 1(b)). Conversion coefficients were obtained using the ESTAR database (Berger 2005a) averaging $(S_{col}/\rho)^{m}_{w}$ values with energies between 0.010 MeV and 1.5 MeV since electron spectra were not simulated for the evaluated clinical case.

3. Results

3.1. Mean photon energy

Mean photon energies obtained using segmented tissue compositions and mass densities from a calibrated CT image (phantom III) are shown in two planes of the head and neck geometry in figures 3(a) and (b). Histograms of the number of voxels as function of mean energy were obtained for the three phantom models, considering the whole CT-defined patient volume excluding regions with air (figure 3(c)). The mean photon energy distribution ranges from 222 keV up to 356 keV.

Small differences in mean energy are observed between the three phantoms (figure 3(c)). A mean energy shift towards lower photon energies was observed for the simulation of

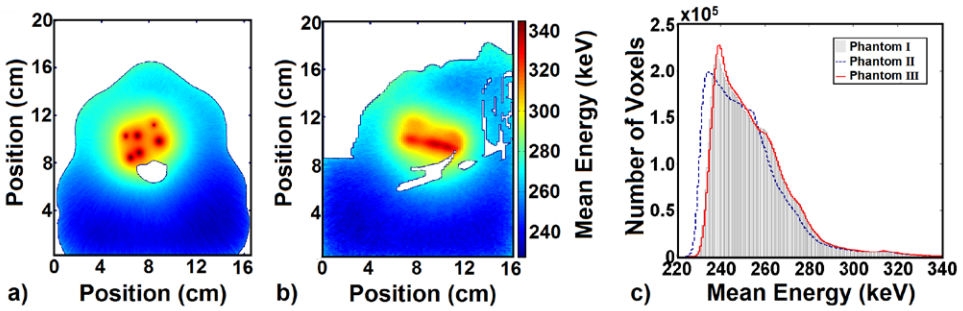

Figure 3. Axial (a) and sagittal (b) spatial distribution of the mean photon energy distribution for the evaluated head and neck case and mean energy-volume histograms (c) for all voxels scored over the whole CT volume, excluding air voxels. Uncertainty <4% for all voxels (Type A $\pm 1\sigma$).

phantom II compared to phantom I (figure 3(c)) while hardly any difference could be observed between phantoms I and III. Figure 4 shows the local mean photon energy ratios to investigate this further.

The phantom II has a mean mass density of $(1.04 \pm 0.03)\,\mathrm{g\,cm^{-3}}$ ($\pm 1\sigma$), excluding air regions, and a maximum mass density of $2.9\,\mathrm{g\,cm^{-3}}$. Higher mass densities resulted in a shift towards lower energies when compared against phantom I (figure 4(a)). On the other hand, bone chemical composition acts as a photon fluence hardener (due to higher Z components) by the higher preferential absorption of low energy photons due to the photo-electric effect. This can be seen in the regions behind the bone (III) in figure 4(b), which have higher mean photon energies than the ones obtained using a water (II) with the same mass densities. The photon fluence hardening effect compensates, for this specific case, the effect produced by higher mass densities leading to small mean energy differences between the results obtained for phantoms I and III (figures 3(c) and 4(c)).

3.2. Photon spectrum

The photon spectrum emitted from the stainless steel source capsule (averaged over all angles of a single source) and the photon spectrum at two evaluated voxels for which the minimum (P13) and the maximum (P9) mean photon energy values were obtained are shown in figure 5. P9 is inside the target volume at 0.4 cm from the nearest dwell position and at an average distance from the dwell positions of 1.4 cm whilst P13 is at 7.1 cm from the nearest dwell position and at an average distance from the dwell positions of 8.5 cm with a dose rate approximately 45 times smaller than at P9. The photon spectra for P13 obtained with the three phantoms are very similar showing hardly any visible differences in the low energy range due to the higher absorption of low energy photons by bone with phantom III.

3.3. CPE conditions and the validity of using MC track-length estimator

$D_{\mathrm{m,m}}$ values obtained using a track length estimation tally show good agreement with values obtained using a pulse height tally with no systematic differences. Therefore, CPE can be assumed and the track-length estimator considered to be accurate for the voxel dimension ($0.39 \times 0.39 \times 2.00\,\mathrm{mm^3}$) used here. The mean of the ratio between the dose distribution

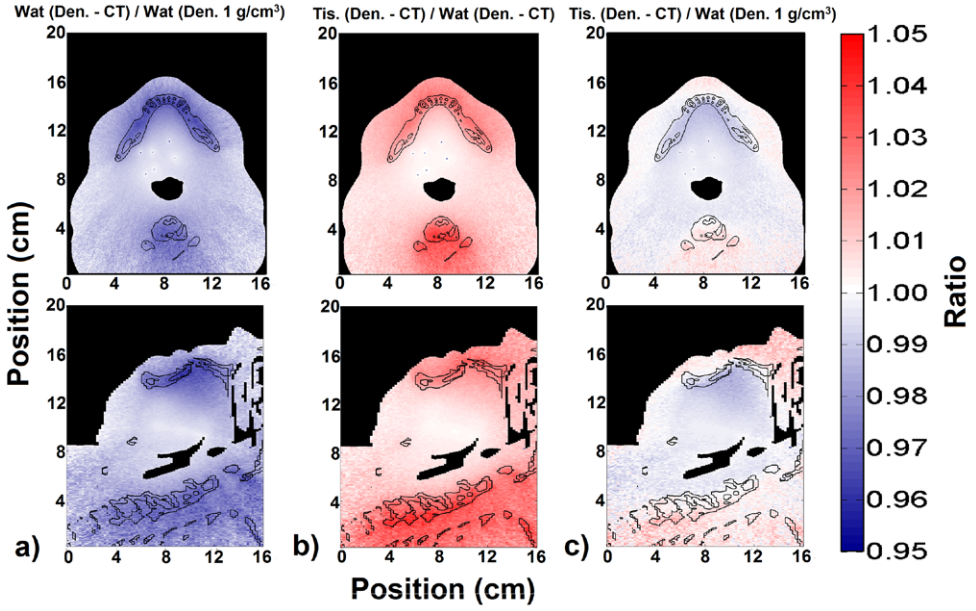

Figure 4. Axial and sagittal view of the mean photon energy ratio: (a) phantom II over phantom I. This shows the density effect since both phantoms consist of only water; (b) phantom III over phantom II. This shows the composition effect since all voxels have the same mass densities; (c) phantom III over phantom I. This shows the atomic number and density effects that approximately compensate each other. Contours in black represent bone tissue.

obtained using F6 and F8, is 1.000 $\pm$ 0.013 (1σ) indicating that differences are due to statistical noise.

The maximum uncertainty is <1%, Type A $\pm 1\sigma$, for all values obtained with a track length tally and are up to 4.5% for the pulse height tally. The simulation time for the latter, necessary to obtain uncertainty values equivalent to the ones obtained using track-length scoring, would be around 1000 times longer when including electron transport without variance reduction techniques. All the results described below were obtained using a track length tally.

3.4. $D_{m,m}$ and $D_{w,m}$

The results obtained for some tissues (prostate, breast, skin, bladder, cartilage) were not described for brevity since they do not differ significantly from the ones obtained with muscle and adipose tissue.

3.4.1. $D_{w,m}$ (SCT) $D_{w,m}$ (SCT) values were calculated by multiplying the $D_{m,m}$ simulated results by the values shown in table 1. An energy-spectrum averaged value is a good approach since $(S_{col}/\rho)^{m}_{w}$ vary slowly as function of electron energy; for bone it goes from 0.868 up to 0.888 for monoenergetic sources with 20 keV and 300 keV, respectively (figure 1(b)). Such small differences indicate that average values can be employed without significant added uncertainties, see also figure 1(b).

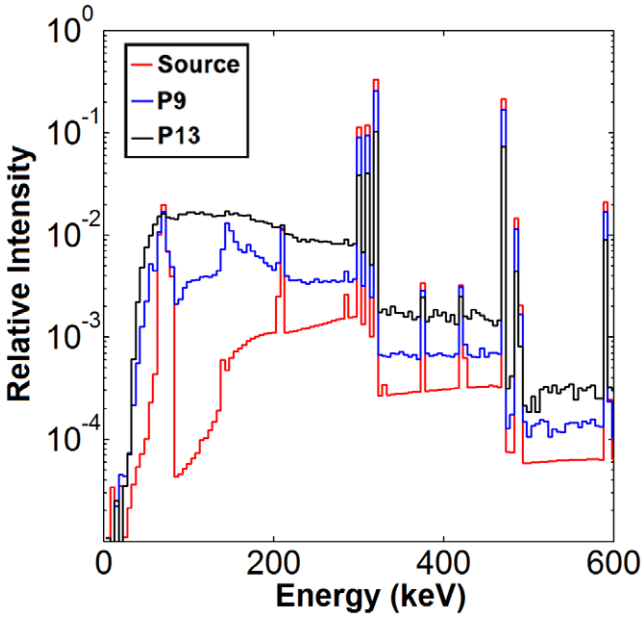

Figure 5. Photon spectrum emitted from the stainless steel capsule (averaged over all angles of a single source) and at two evaluated voxels, P9 and P13. Values were normalized for the total fluence in their respective voxel and grouped using 5 keV energy bins. Most of the photons from the source are concentrated on the peaks of the spectrum that represent the primary photons. Only values between 0 and 600 keV were displayed to highlight differences in this region.

Table 1. The conversion coefficients from $D_{m,m}$ to $D_{w,m}$ (SCT) obtained using average mass stopping power ratios for some materials evaluated in this study.

	Lung	Adip. tissue	Muscle	Mandible	Bone	Teeth
$(S/\rho)_w^m$	0.992	1.020	0.992	0.963	0.883	0.853

3.4.2. $D_{w,m}$ (LCT) Unlike $D_{w,m}$ (SCT) results, ratios between $D_{m,m}$ and $D_{w,m}$ (LCT) vary significantly with the photon spectrum and hence with position in the patient/phantom, in particular for some materials. Figure 6 shows the ratio between $D_{m,m}$ and $D_{w,m}$ (LCT) obtained for the clinical case. Ratios are approximately constant for adipose tissue and muscle, with a small dependence on the photon spectrum of each voxel. Differences can be significant for regions assigned as bone tissue with dose ratios ranging from 1.00 up to 1.14 (maximum difference observed in a voxel not shown in figure 6).

Variations in the photon spectrum may lead to differences between $D_{m,m}$ and $D_{w,m}$ (LCT) for the same material of up to >15%, as shown in figure 7 while for $D_{m,m}$ and $D_{w,m}$ (SCT) the ratios are nearly invariant (see table 1 and figure 1(b)). Different phantom models for the same patient also lead to small differences, due to the slightly smaller low photon energy intensities for phantom III. Although differences in the photon spectrum are not clearly visible for the voxel P13, the ratio between $D_{m,m}$ and $D_{w,m}$ (LCT) for bone is 1.121, 1.142 and 1.106 for the spectrums obtained in phantoms I, II and III, respectively.

The ratio between $D_{m,m}$ and $D_{w,m}$ (LCT) values obtained using the full photon spectrum and the mean photon energy, as a function of the mean photon energy in each one of the 25

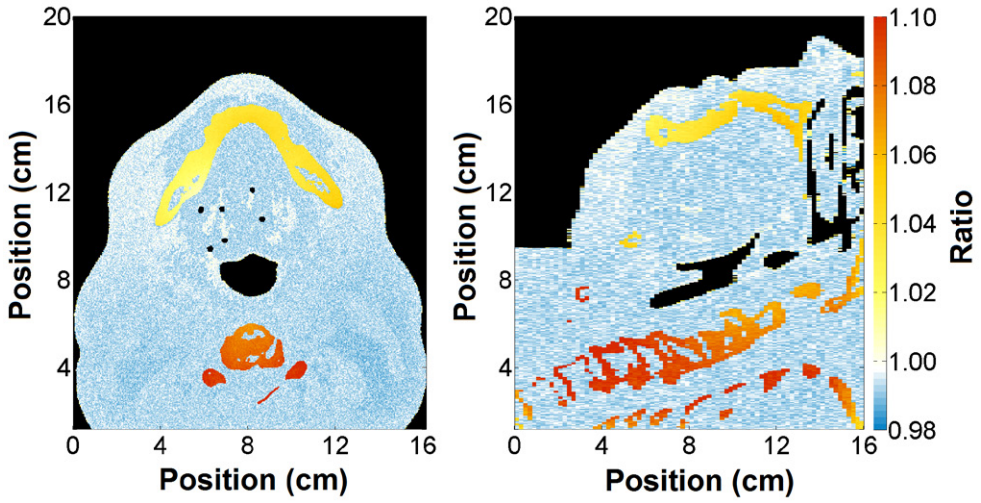

Figure 6. Ratio ($D_{m,m}$ / $D_{w,m}$ (LCT)) obtained using a track length estimator tally. Uncertainty <1% for all points inside of the CT volume (Type A $\pm 1\sigma$). Regions with air were excluded.

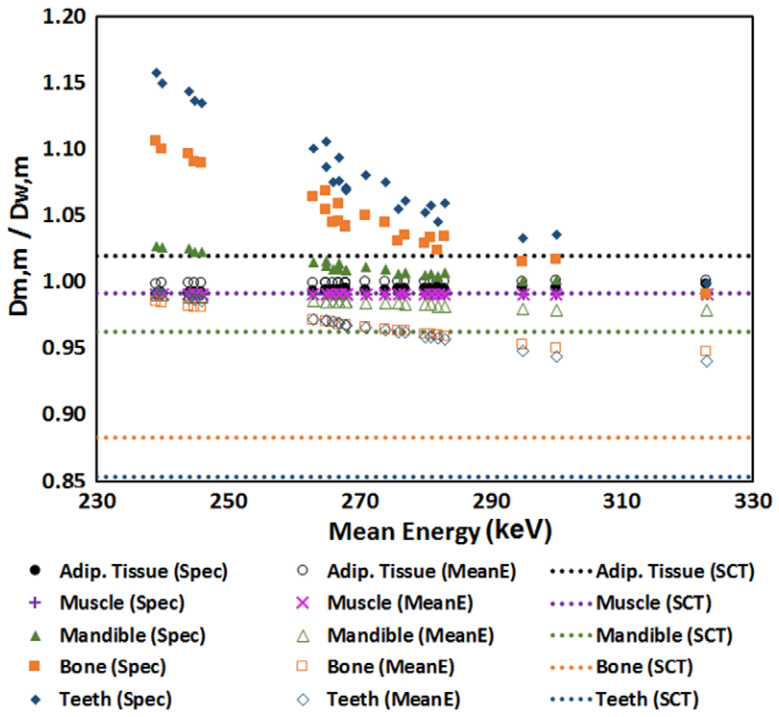

Figure 7. Ratio between $D_{m,m}$ and $D_{w,m}$ (LCT) obtained with the photon spectrum and with the mean photon energy scored (phantom III) for the 25 evaluated voxels (figure 2). Mandible corresponds to mandible spongiosa from ICRP Report 110 (ICRP 2009). Uncertainty is <1% for all dose ratios (Type A $\pm 1\sigma$).

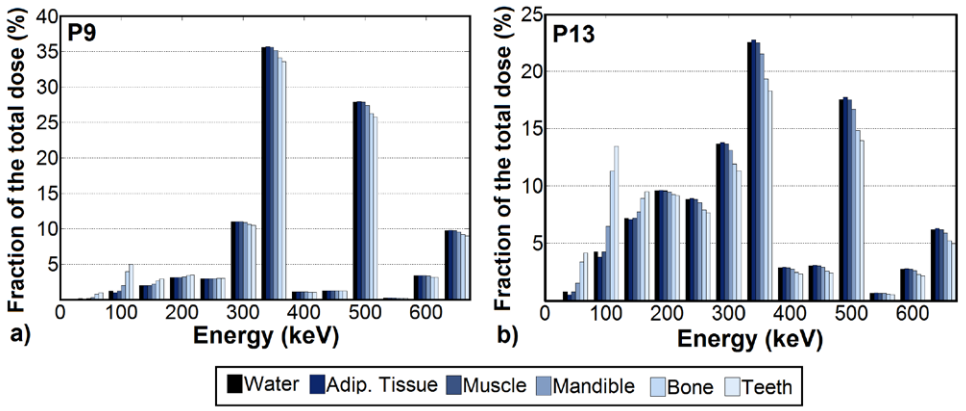

Figure 8. Contribution of various parts of the photon spectrum to the total dose at two evaluated voxels, P9 and P13. Photons with energies greater than 650 keV contribute less than 0.3% of the total dose. Uncertainty <1% for the total dose (Type A $\pm 1\sigma$). Mandible corresponds to mandible spongiosa from ICRP Report 110 (ICRP 2009).

selected voxels, is shown in figure 7. The ratio between $D_{m,m}$ and $D_{w,m}$ (SCT) is approximately constant and was added for illustrative purposes. The ratio $D_{w,m}$ (SCT)/$D_{m,m}$ for teeth is approximately 0.853 whilst the value of $D_{w,m}$ (LCT)/$D_{m,m}$ is up to 1.158 which represents the largest difference observed for the evaluated points.

The ratio between $D_{m,m}$ and $D_{w,m}$ (LCT) varies considerably over the patient volume for some materials due to the photon fluence softening (energy decrease) with distance from the source that increases the number of low energies photons for which $(\mu_{en}/\rho)^{m}_{w}$ values are more relevant. The contribution from low energy photons to the total dose is more relevant in some regions (figure 8), with less than 6% of the total dose coming from energies less than 100 keV for all materials at P9. This fraction increases for all materials at P13 reaching up to 17.6% of the total dose for teeth. Muscle, adipose tissue, and water showed a similar behavior with the dose contribution from photons with energies lower than 100 keV increasing around 3.5% between P9 and P13 whilst it increased 5.7%, 9.9% and 11.6% for mandible spongiosa, bone and teeth, respectively.

4. Discussion

The mean photon energies illustrate the effect of the different phantom models employed for the same patient due to beam softening or hardening (figure 4). Mean photon energy differences due to the three different phantoms are within ±5% and would not result in significant differences in conversion factors between $D_{m,m}$ and $D_{w,m}$ (LCT) for the mean energy range (222–356 keV) since $(\mu_{en}/\rho)^{m}_{w}$, within this energy range, is close to 1 for the evaluated human tissues. However, these values should not be employed to obtain conversion factors between $D_{m,m}$ and $D_{w,m}$ (LCT) since mean photon energy values may lead to wrong results for some tissues (e.g. mandible spongiosa, bone and teeth).

The correct tissue and mass density assignment is relevant since small differences in the low energy photon intensities can lead to significant differences in the $D_{m,m}$ and $D_{w,m}$ (LCT) values for some materials (figure 6). Although tissue segmentation is necessary to obtain $D_{w,m}$ values, a simpler approach using a water phantom with densities from CT (phantom II) may provide results for $D_{w,m}$ (LCT) and $D_{m,m}$ in the case of soft tissues similar to those obtained

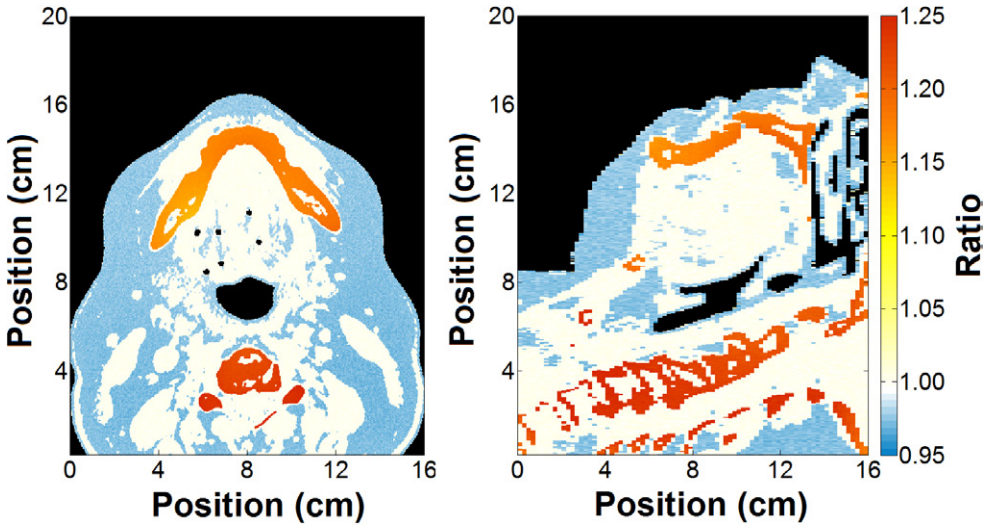

Figure 9. Ratio between conversion coefficients ($D_{w,m}$(LCT)/$D_{w,m}$(SCT)). Uncertainty <1% for all points inside of the CT volume (Type A $\pm 1\sigma$).

using proper tissue composition (phantom III). The three different phantoms produced very similar photon spectra. The mean of the ratios between $D_{w,w-\text{phantom II}}$ and $D_{w,m-\text{phantom III}}$ is 0.9980 $\pm$ 0.0002 (1σ) within the CT volume. A similar approach used for high energy (4–18 MV) photon beams showed that water with relative electron mass densities of tissues produces $D_{w,w}$ values much closer to $D_{m,m}$ values obtained with MC codes than values converted using mass stopping-power ratios (Ma and Li 2011). This result is associated with Compton scattering, which is the dominant mode of interaction for EBRT energies and depends mainly on the electronic density of materials (Ma and Li 2011). For the ^{192}Ir photon spectrum Compton scattering is the most frequent interaction type for all human tissues at most of the energies encountered in the current patient geometry. However, the percentage of low energy photons may be more significant in some regions (figure 8) increasing the occurrence of photoelectric effect for which tissue composition (high atomic number materials e.g. bone and teeth) is relevant. It explains the small differences between $D_{w,m}$ and $D_{m,m}$ (LCT) for soft tissues in all regions and differences varying with the photon spectrum at each voxel for some tissues such as bone and teeth (figure 7).

Different approaches (SCT or LCT) can lead to similar results or relevant differences in $D_{w,m}$. The SCT and LCT approaches are almost equivalent for some tissues such as muscle for which the conversion factors is 0.992 (SCT—table 1) and 0.991 (LCT—figure 7). However, differences are significant for some tissues such as adipose tissue and bone (figure 9). Conversion factors for adipose tissues (LCT) range from 0.990 to 0.998 whilst the SCT conversion factor is 1.020 so the ratio (LCT/SCT) is between 0.97 and 0.98 depending on the photon spectrum. The ratio between conversion factors (LCT/SCT) for bone shows wider range ranging from 1.13 up to 1.29 and up to 1.36 for teeth. Large differences observed for some tissues (mandible spongiosa, bone and teeth) are expected since $(\mu_{en}/\rho)^{m}_{w}$ is greater than 1 (for low energy photons) for these materials whilst $(S/\rho)^{m}_{w}$ is less than 1 for the same materials (figure 1). These differences make it essential to compare dose distributions with the same reporting quantity, which must be taken into account for different treatment modalities. SCT is commonly employed in EBRT and the LCT adoption for brachytherapy would lead to dose differences due to the reporting quantity. In head and neck cases, dose to the bony mandible

is often of interest as this is considered an organ at risk. Great caution in which dose quantity is reported and how to compare dose values with earlier clinical experience is of the utmost importance in this and similar cases.

The correct tissue segmentation is necessary to calculate correction factors between $D_{m,m}$ and $D_{w,m}$ since miss-assignments can lead to differences, e.g. assignment of muscle to adipose tissue voxels leads to a 3% difference and even higher differences for bone or a few other tissues (SCT—table 1). Therefore, converting $D_{m,m}$ into $D_{w,m}$ involves additional uncertainties.

Cavity theory based conversion factors are also relevant for experimental dosimetry (Li *et al* 2000, Araki *et al* 2013, Lucas *et al* 2014). The signal from a detector depends on the absorbed dose to the detector material which may need to be taken into account if a detector has been calibrated for $D_{w,w}$ in another beam quality than that used for measurements (like calibration in ^{60}Co or 6 MV which is recommended in TG43 (Nath *et al* 1995, Rivard *et al* 2004) for measurements around brachytherapy sources). The effect of different photon spectra on the dosimeter is also a relevant issue and was the subject of several studies with different dosimeters, e.g. termoluminescent dosimeters (TLD) (Nunn *et al* 2008, Tedgren *et al* 2011, Massillon *et al* 2014), due to their intrinsic response, and MOSFETs (Ehringfeld *et al* 2005, Zilio *et al* 2006, Reniers *et al* 2012), due their composition. Differences around 100 keV in the mean photon energies due to medium attenuation for a ^{192}Ir source can represent an over response around 60% for MOSFET dosimeters. (Reniers *et al* 2012) The MOSFET detector is of interest for clinical routine measurements due to convenience in handling and their fast, direct reading results. The problem of their large energy-dependence could be overcome by scoring the photon energy spectrum at the dosimeter positions during in-vivo measurements (similar to the 25 reference points evaluated in this study), thus accounting for all dwell positions, different densities and tissue composition. This way, more accurate energy correction factors would be obtained for energy dependent dosimeters.

5. Conclusion

For HDR brachytherapy with the ^{192}Ir isotope the mean photon energy changes within ± 5% whilst the photon spectrum changes considerably inside the patient as function of distance to implant and depending on the patient/phantom material composition. The low energy photon contribution to the total dose is higher in regions away from the implant. The results obtained show that differences between $D_{m,m}$ and $D_{w,m}$ (SCT or LCT) can be negligible (<1%) for some tissues such as muscle and significant for other tissues with differences up to 14% for bone in the evaluated head and neck case. The dose conversion approach (SCT or LCT) leads to significant differences since materials with $(\mu_{en}/\rho)^{m}_{w}$ greater than 1 may have $(S/\rho)^{m}_{w}$ less than 1 or vice versa (figure 1). Therefore differences between conversion factors (LCT and SCT) are up to 29% for bone and 36% for teeth. It is essential that brachytherapy studies explicitly mention which dose reporting quantity has been used ($D_{m,m}$, $D_{w,m}$ (LCT), or $D_{w,m}$ (SCT)). Of extra importance is to be aware that in some materials and locations, the difference between $D_{w,m}$(LCT), $D_{w,m}$ (SCT) and $D_{m,m}$ are substantial. More studies on this issue are needed in brachytherapy.

Acknowledgments

This work was partially supported by *Fundação de Amparo à Pesquisa do Estado de São Paulo* (FAPESP), grant numbers 2011/01913-4, 2011/23765-7 and 2011/22778-8. ÅCT is grateful to acknowledge the Swedish Cancer Foundation, grant number CF 14 064.

References

Afsharpour H *et al* 2012 ALGEBRA: algorithm for the heterogeneous dosimetry based on GEANT4 for brachytherapy *Phys. Med. Biol.* **57** 3273

Ahnesjo A 1989 Collapsed cone convolution of radiant energy for photon dose calculation in heterogeneous media *Med. Phys.* **16** 577–92

Andreo P 2015 Dose to 'water-like' media or dose to tissue in MV photons radiotherapy treatment planning: still a matter of debate *Phys. Med. Biol.* **60** 309–37

Araki F *et al* 2013 Measurement of absorbed dose-to-water for an HDR (192)Ir source with ionization chambers in a sandwich setup *Med. Phys.* **40** 092101

Baglin C M 2012 Nuclear data sheets for $A = 192$ *Nucl. Data Sheets* **113** 1871–2111

Ballester F *et al* 2009 Evaluation of high-energy brachytherapy source electronic disequilibrium and dose from emitted electrons *Med. Phys.* **36** 4250–6

Beaulieu L *et al* 2012 Report of the Task Group 186 on model-based dose calculation methods in brachytherapy beyond the TG-43 formalism: current status and recommendations for clinical implementation *Med. Phys.* **39** 6208–36

Berger M J, Coursey J S, Zucker M A and Chang J 2005a *ESTAR, PSTAR, and ASTAR: Computer Programs for Calculating Stopping-Power and Range Tables for Electrons, Protons, and Helium Ions (Version 1.2.3)* (Gaithersburg, MD: NIST)

Berger M J, Hubbell J H, Seltzer S M, Chang J, Coursey J S, Sukumar R, Zucker D S, and Olsen K 2005b *XCOM: Photon Cross Section Database (Version 1.3)* (Gaithersburg, MD: NIST)

Carlsson Tedgren Å and Ahnesjo A 2000 The collapsed cone superposition algorithm applied to scatter dose calculations in brachytherapy *Med. Phys.* **27** 2320–32

Carlsson Tedgren Å and Ahnesjo A 2003 Accounting for high Z shields in brachytherapy using collapsed cone superposition for scatter dose calculation *Med. Phys.* **30** 2206–17

Carlsson Tedgren Å and Ahnesjo A 2008 Optimization of the computational efficiency of a 3D, collapsed cone dose calculation algorithm for brachytherapy *Med. Phys.* **35** 1611–8

Carlsson Tedgren Å and Alm Carlsson G 2013 Specification of absorbed dose to water using model-based dose calculation algorithms for treatment planning in brachytherapy *Phys. Med. Biol.* **58** 2561–79

Carron N J 2006 *An Introduction to the Passage of Energetic Particles through Matter* (Boca Raton, FL: Taylor and Francis)

Chadwick M B 2012 ENDF nuclear data in the physical, biological, and medical sciences *Int. J. Radiat. Biol.* **88** 10–4

Chetty I J *et al* 2007 Report of the AAPM Task Group No. 105: Issues associated with clinical implementation of Monte Carlo-based photon and electron external beam treatment planning *Med. Phys.* **34** 4818–53

Daskalov G M, Loffler E and Williamson J F 1998 Monte Carlo-aided dosimetry of a new high dose-rate brachytherapy source *Med. Phys.* **25** 2200–8

Ehringfeld C *et al* 2005 Application of commercial MOSFET detectors for in vivo dosimetry in the therapeutic x-ray range from 80 kV to 250 kV *Phys. Med. Biol.* **50** 289–303

Enger S A *et al* 2012 Dose to tissue medium or water cavities as surrogate for the dose to cell nuclei at brachytherapy photon energies *Phys. Med. Biol.* **57** 4489–500

Fonseca G P *et al* 2014 A medical image-based graphical platform-features, applications and relevance for brachytherapy *Brachytherapy* **13** 632–9

Goorley J T *et al* 2013 Initial MCNP6 release overview—MCNP6 version 1.0 (Los Alamos, NM: Los Alamos National Laboratory)

Hughes H G 2013 *Recent Developments in Low-Energy Electron/Photon Transport for MCNP6* (Los Alamos, NM: Los Alamos National Laboratory)

ICRP 2009 Adult reference computational phantoms *ICRP Publication* 110 (Oxford: Elsevier)

Landry G *et al* 2011 The difference of scoring dose to water or tissues in Monte Carlo dose calculations for low energy brachytherapy photon sources *Med. Phys.* **38** 1526–33

Li Z, Fan J J and Palta J R 2000 Experimental measurements of dosimetric parameters on the transverse axis of a new ^{125}I source *Med. Phys.* **27** 1275–80

Lindborg L *et al* 2013 Lineal energy and radiation quality in radiation therapy: model calculations and comparison with experiment *Phys. Med. Biol.* **58** 3089–105

Liu H H, Keall P and Hendee W R 2002 D_m rather than D_w should be used in Monte Carlo treatment planning *Med. Phys.* **29** 922–4

Lloyd S A and Ansbacher W 2013 Evaluation of an analytic linear Boltzmann transport equation solver for high-density inhomogeneities *Med. Phys.* **40** 011707

Lucas P A *et al* 2014 Using LiF:Mg,Cu,P TLDs to estimate the absorbed dose to water in liquid water around an ^{192}Ir brachytherapy source *Med. Phys.* **41** 011711

Ma C M and Li J 2011 Dose specification for radiation therapy: dose to water or dose to medium? *Phys. Med. Biol.* **56** 3073–89

Massillon J L G *et al* 2014 Influence of phantom materials on the energy dependence of LiF:Mg,Ti thermoluminescent dosimeters exposed to 20–300 kV narrow x-ray spectra, ^{137}Cs and ^{60}Co photons *Phys. Med. Biol.* **59** 4149–66

Mikell J K *et al* 2013 Commissioning of a grid-based Boltzmann solver for cervical cancer brachytherapy treatment planning with shielded colpostats *Brachytherapy* **12** 645–53

Nath R *et al* 1995 Dosimetry of interstitial brachytherapy sources: recommendations of the AAPM Radiation Therapy Committee Task Group No. 43. American Association of Physicists in Medicine *Med. Phys.* **22** 209–34

Nunn A A *et al* 2008 LiF:Mg,Ti TLD response as a function of photon energy for moderately filtered x-ray spectra in the range of 20–250 kVp relative to ^{60}Co *Med. Phys.* **35** 1859–69

Petrokokkinos L *et al* 2011 Dosimetric accuracy of a deterministic radiation transport based ^{192}Ir brachytherapy treatment planning system. Part II: Monte Carlo and experimental verification of a multiple source dwell position plan employing a shielded applicator *Med. Phys.* **38** 1981–92

Poon E *et al* 2008 BrachyGUI: an adjunct to an accelerated Monte Carlo photon transport code for patient-specific brachytherapy dose calculations and analysis *J. Phys.: Conf. Ser.* **102** 012018

Reniers B *et al* 2012 *In vivo* dosimetry for gynaecological brachytherapy using a novel position sensitive radiation detector: feasibility study *Med. Phys.* **39** 1925–35

Rivard M J, Beaulieu L and Mourtada F 2010a Enhancements to commissioning techniques and quality assurance of brachytherapy treatment planning systems that use model-based dose calculation algorithms *Med. Phys.* **37** 2645–58

Rivard M J *et al* 2004 Update of AAPM Task Group No. 43 Report: a revised AAPM protocol for brachytherapy dose calculations *Med. Phys.* **31** 633–74

Rivard M J *et al* 2006 Calculated and measured brachytherapy dosimetry parameters in water for the Xoft Axxent x-ray Source: an electronic brachytherapy source *Med. Phys.* **33** 4020–32

Rivard M J *et al* 2010b Influence of photon energy spectra from brachytherapy sources on Monte Carlo simulations of kerma and dose rates in water and air *Med. Phys.* **37** 869–76

Rivard M J, Venselaar J L and Beaulieu L 2009 The evolution of brachytherapy treatment planning *Med. Phys.* **36** 2136–53

Russell K R, Tedgren A K and Ahnesjo A 2005 Brachytherapy source characterization for improved dose calculations using primary and scatter dose separation *Med. Phys.* **32** 2739–52

Goorley M J *et al* 2012 Initial MCNP6 release overview *Radiat. Transp. Protect.* **180** 298–315

Taylor R E and Rogers D W 2008 EGSnrc Monte Carlo calculated dosimetry parameters for ^{192}Ir and ^{169}Yb brachytherapy sources *Med. Phys.* **35** 4933–44

Taylor R E P, Yegin G and Rogers D W O 2007 Benchmarking brachydose: voxel based EGSnrc Monte Carlo calculations of TG-43 dosimetry parameters *Med. Phys.* **34** 445–57

Tedgren A C *et al* 2011 Response of LiF:Mg,Ti thermoluminescent dosimeters at photon energies relevant to the dosimetry of brachytherapy (<1 MeV) *Med. Phys.* **38** 5539–50

Thomson R *et al* 2010 Sci—Sat AM(2): brachy—05: fast Monte Carlo dose calculations for brachytherapy with brachydose *Med. Phys.* **37** 3910

Thomson R M, Tedgren A C and Williamson J F 2013 On the biological basis for competing macroscopic dose descriptors for kilovoltage dosimetry: cellular dosimetry for brachytherapy and diagnostic radiology *Phys. Med. Biol.* **58** 1123–50

Wang R and Li X A 2002 Dose characterization in the near-source region for two high dose rate brachytherapy sources *Med. Phys.* **29** 1678–86

White M C 2003 *Photoatomic Data Library MCPLIB04: a New Photoatomic Library Based On Data from ENDF/B-VI Release 8* (Los alamos, NM: Los Alamos National Laboratory)

White S A *et al* 2014 Comparison of TG-43 and TG-186 in breast irradiation using a low energy electronic brachytherapy source *Med. Phys.* **41** 061701–12

Williamson J F 1987 Monte Carlo evaluation of kerma at a point for photon transport problems *Med. Phys.* **14** 567–76

Zilio V O *et al* 2006 Absolute depth-dose-rate measurements for an ^{192}Ir HDR brachytherapy source in water using MOSFET detectors *Med. Phys.* **33** 1532–9